4. RESULTS

The main goal of this work was to study functionally relevant complexes of the 30S ribosomal subunit with various ligands as a way to improve the *Thermus thermophilus* 30S crystals and understand the function of the used ligands. These ligands include cDNA oligonucleotides (section 4.1) that can bind specifically to the 16S rRNA; the initiation factor 3 (section 4.2) and specifically its C-terminal domain, and two antibiotics (section 4.3.2), tetracycline and edeine, known to block the A-site tRNA binding and the initiation process, respectively.

4.1 c-DNA

Over a dozen of oligonucleotides complementary to specific regions of the 16S rRNA were synthesised and their binding to the 30S subunit tested in solution. The length of the oligonucleotides was designed having in mind the stability of the expected hybrid double helix (Figure 4). The oligonucleotides were directed against 16S rRNA regions known to be exposed and therefore accessible to the binding of short oligonucleotides in *E. coli* 16S rRNA (Oakes et al., 1986; Hill et al., 1988; Ricker and Kaji, 1991; Alexander et al., 1994; Wang et al., 1999).

4.1.1 Analysis of the binding of the oligonucleotides to the 30S in solution

The first step was to analyse if the oligonucleotides from Figure 4 were able to bind to the complementary region in the 16S rRNA of the *T. thermophilus*. Therefore, they were phophorylated at the 5' end using γ-ATP and the degree of binding and the stability of the binding was checked by the amount of labelled oligonucleotide bound to the 30S subunit after sucrose gradient centrifugation (see sections 3.4.2 and 3.3.4).
It was found that the *T. thermophilus* 16S rRNA regions corresponding to nucleotides 182-197 (placed on the bottom of the 30S subunit), 541-557 and 763-778 (on the platform), 942-958, 1179-1195 and 1242-1258 (on the head) were not accessible to the oligonucleotides, at least in the conditions used during these experiments, since no significant binding could be detected. The region corresponding to nucleotides 466-482 (on the shoulder) was partially accessible showing a binding of 50% (1 pmol oligonucleotide / 2 pmol T30S) could be detected, whereas the region corresponding to the 3' end (nucleotides 1504-1518) was totally accessible since stoichiometric binding could be detected. In the region corresponding to the decoding region (nucleotides 1371-1389) a binding between 24 and 100% was detected depending from the length of the oligonucleotide used. The shortest oligonucleotides showed the lower binding extent probably due to the lower stability of the cDNA:RNA hybrid (Table 1).

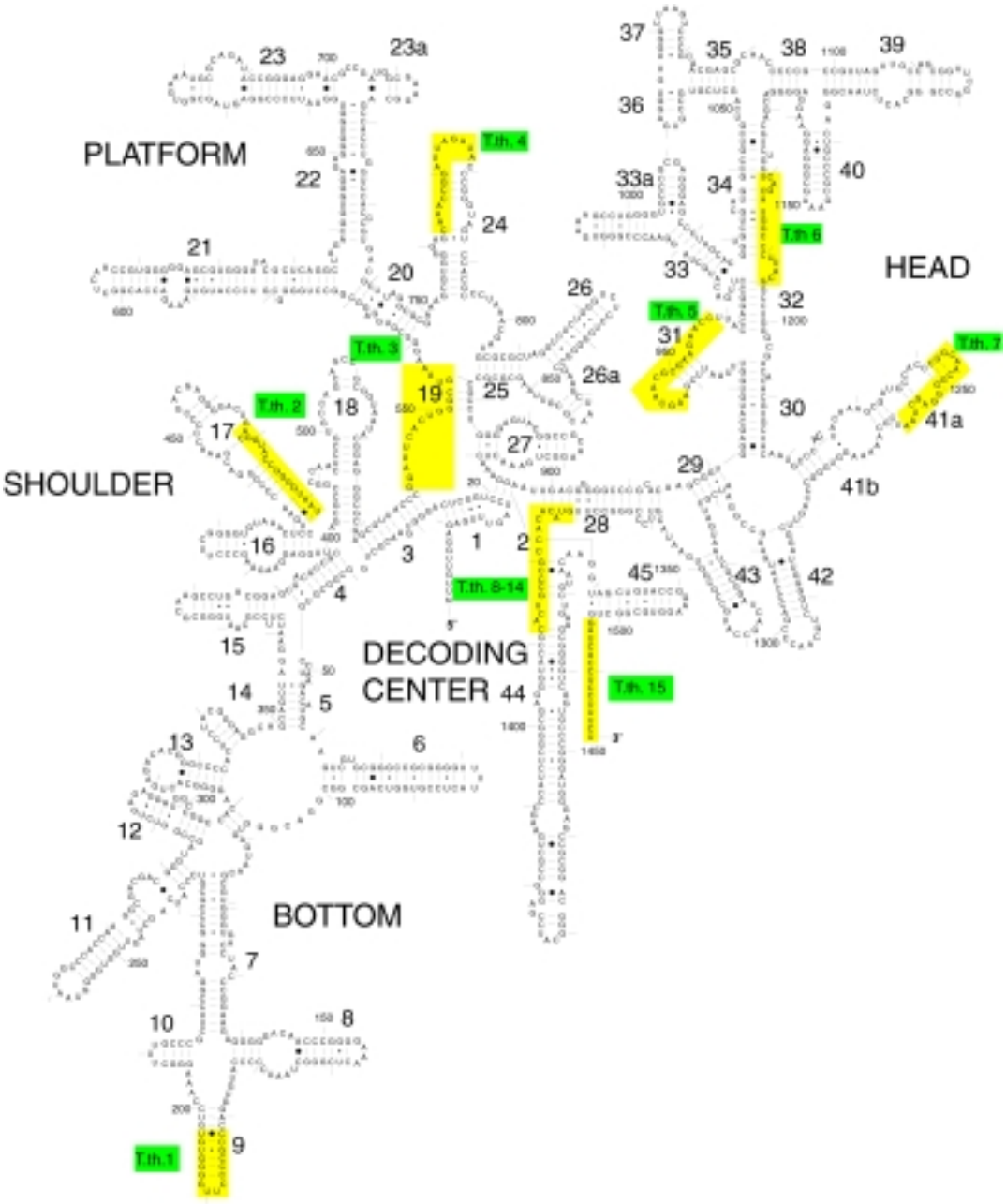

Figure 4. *Secondary structure of the 16S rRNA from T. thermophilus. (Gutell et al., 1999).*

In the yellow boxes are marked the sequences to which the oligonucleotides used in this study are complementary.

The next step was to modify the oligonucleotides that bind to the *T. thermophilus* 16S rRNA in almost stochiometric ratio introducing at least one guanosine at one of the extremes and the binding in solution was tested again. Subsequently, guanosine was substituted with 6-thio-deoxiguanosine (6-thio-dG) to which heavy metal atoms or heavy metal cluster can bind. Toward this goal a new labelling method was developed (see sections 3.4.5, 3.4.6 and 3.4.7).
First, the oligonucleotides hybridising to the 3' end of the *T. thermophilus* 16S rRNA and to the decoding region, which showed the best binding, were synthesised with a non-complementary tail of one to three deoxi-guanosines attached to the 3' end, to the 5' end or to both extremes, and the binding in solution was tested again. In most of the cases the binding was not drastically affected due to the deoxi-guanosine tail (Table 1). Therefore, the oligonucleotides were then synthesised substituting at least one of the deoxi-guanosine residue for 6-thio-dG, which can covalently bind TAMM, a tetra-mercury complex (Figure 5). The TAMM molecule has a dual chemical nature, since it has four reactive mercury atoms it is possible that the mercury atoms bridge with some other regions in the 30S or form TAMM dimers. Therefore, special efforts were made to minimise the chemical reactivity of the TAMM in such a way that the formation of intermolecular cross-link was reduced to a minimum. Hence, statistically, three of the four mercury atoms in the TAMM molecule were blocked with [^{35}S]-cysteine. The use of [^{35}S]-cysteine as blocking reagent had also the advantage that allowed us to quantify the binding of the TAMM labelled oligonucleotides to the 30S subunit.

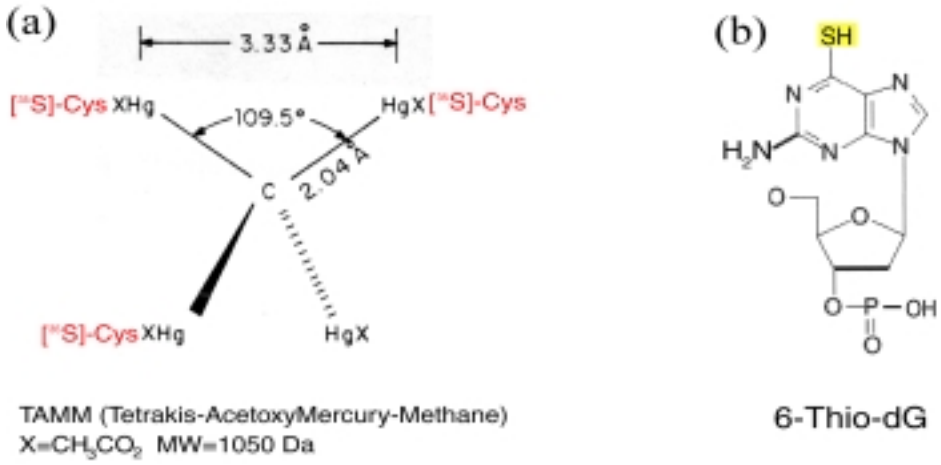

Figure 5. *TAMM and 6-thio-deoxiguanosine.*

(a) Three out of the four the mercury atoms of the TAMM were blocked with [^{35}S]-Cys to prevent intermolecular cross-linking and to be able to follow the labelling reaction. (b) The 6-thio-dG used to synthesise the modified oligonucleotides provides SH groups to which TAMM can bind.

One feature of the oligonucleotides containing 6-thio-dG is the presence in the UV spectra of a characteristic peak at 340 nm. This peak disappears completely once the SH group is blocked, in this case by the binding of TAMM.
In Figure 6 are shown the spectra of one of the oligonucleotides having 6-thio-dG before and after the binding of TAMM. The disappearance of the 340 nm peak, as well as the co-migration of [^{35}S]-cysteine with the oligonucleotide peak, were used as an indication of the TAMM binding.

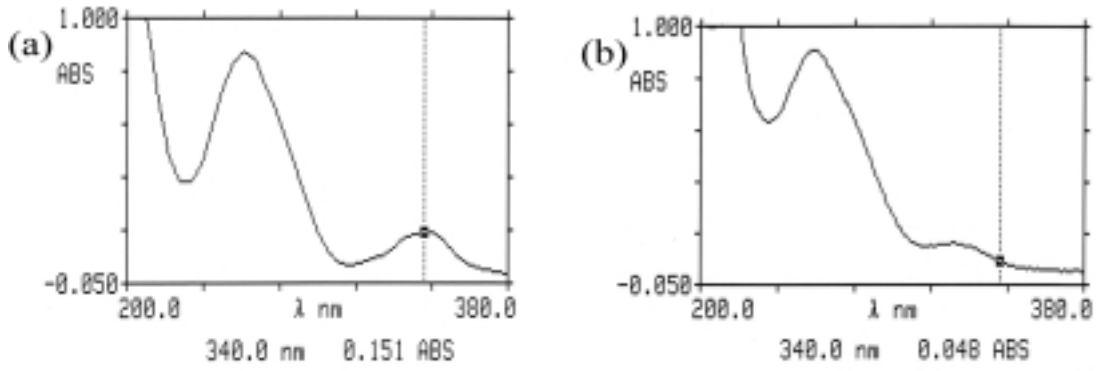

Figure 6. *Spectrum of the 6-thio-dG modified oligonucleotides.*

(a) The peak 340 nm is present in the spectrum of the oligonucleotide before treatment with TAMM. (b) The 340 nm peak disappears from the spectrum after labelling of the oligonucleotide with TAMM.

Another indication for the binding of TAMM to the oligonucleotide was given by the gel shift detected for the labelled oligonucleotide respect to the non-labelled one in urea-acrylamide-gels (Figure 7).

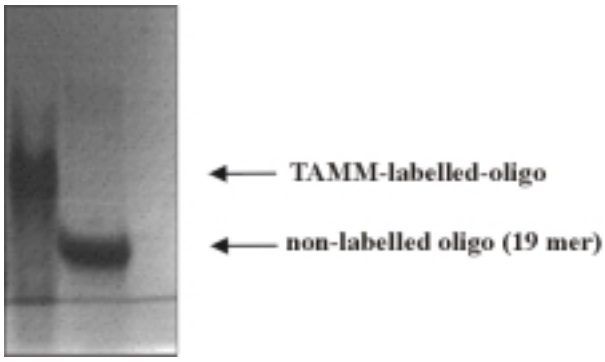

Figure 7. *Urea-acrylamide gel 22% of the modified oligonucleotide.*

The oligonucleotide labelled with TAMM shows a gel retardation respect to the not-labelled one.

The 3[^{35}S]-Cys·TAMM labelled oligonucleotides, obtained as described before, were hybridised to the 16S rRNA in *T. thermophilus* 30S. The binding of the labelled oligonucleotides was checked by the co-migration of the [^{35}S]-cysteine together with the 30S peak (Figure 8).

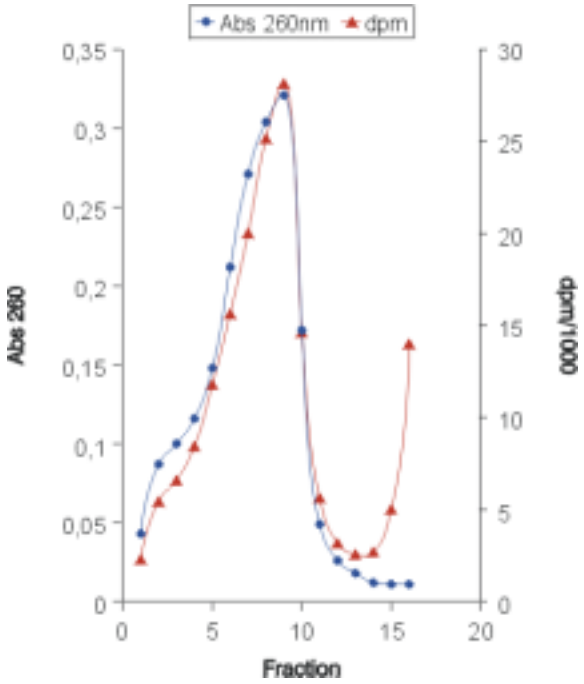

Figure 8. *Gradient binding-assay of the 30S subunit labelled with the oligonucleotides.*
60 pmol of T30S were incubated with a 10-fold excess of a [^{35}S]-Cys·TAMM·oligonulceotide probe. The sample was loaded onto a 5-20% (w/v) sucrose gradient and centrifuged at 22000 rpm for 10 hour at 10°C in a Beckman SW40 rotor. Fractions were collected and monitored for absorbance at 260 nm and radioactivity.

For the TAMM labelled oligonucleotides complementary to the 3' end of the 16S rRNA, binding up to 72% could be detect (oligo T.th. 15k), whereas for the oligonucleotides complementary to the decoding region the binding was up to 85% (oligo T.th. 9c). However, it has to be pointed out that the results obtained here indicate a minimum binding, because the TAMM labelling is done to statistically block three out of the four mercury atoms. Therefore, it could happen that only one or two of the mercury atoms are blocked with [^{35}S]-cysteine. Therefore, the actual binding is at least the reported above.

Table 1. The sequence and the lenght of the oligonucleotides tested, the region of the *Thermus thermophilus* 16S rRNA to which they are complementary and the percentage of their binding in solution are shown.

Name of the oligo	Nucleotide Sequence of the oligo	Length (bases)	Complentary to the 16S rRNA nucleotides	Amount of binding (%)
T.th. 1	5`- ACA CCC CAA GGG GCG G	16	182 - 197	<10
T.th. 2	5`- ATT ACC CCG GTA CCG TC	17	466 - 482	50
T.th. 3	5`- TTA CGC CCA GTG AAT CC	17	541 - 557	< 10
T.th. 4	5`- TAT CTA ATC CGG TTT G	16	763 - 778	< 10
T.th. 5	5`- GGT TCT TCG CGT TGC TT	17	942 - 958	< 10
T.th. 6	5`- CGT AAG GGC CAT GCT GA	17	1179 - 1195	< 10
T.th. 7	5`- TTA GCT CCC CGT TGC CG	17	1242 - 1258	< 10
T.th. 8	5`- TGA CGG GCG GTG TGT AC	17	1371 - 1387	81
T.th. 8a	5`- TGA CGG GCG GTG TGT AC ggg	20	1371 - 1387	68
T.th. 8b	5`- ggg TGA CGG GCG GTG TGT AC	20	1371 - 1387	70
T.th. 9	5`- TGA CGG GCG GTG TGT	15	1373 - 1387	74
T.th. 9a	5`- TGA CGG GCG GTG TGT ggg	18	1373 - 1387	68
T.th. 9b	5`- ggg TGA CGG GCG GTG TGT	18	1373 - 1387	83
T.th. 9c	5`- TGA CGG GCG GTG TGT xxx a	19	1373 - 1387	85
T.th. 9d	5`- xxx TGA CGG GCG GTG TGT	18	1373 - 1387	56
T.th. 10	5`- CGT GAC GGG CGG TGT GT	17	1373 - 1389	61
T.th. 11	5`- CGG GCG GTG TG	11	1374 - 1384	39
T.th. 12	5`- GGG CGG TGT	9	1375 - 1383	24
T.th. 13	5`- TGA CGG GCG GTG T	13	1375 - 1387	56

T.th. 14	5`- ACG GGC GG	8	1378 - 1385	< 10
T.th. 15	5`- AGA AAG GAG GTG ATC	15	1504 - 1518	> 100*
T.th. 15a	5`- g AGA AAG GAG GTG ATC	16	1504 - 1518	> 100*
T.th. 15b	5`- gg AGA AAG GAG GTG ATC	17	1504 - 1518	50
T.th. 15c	5`- ggg AGA AAG GAG GTG ATC	18	1504 - 1518	69
T.th. 15d	5`- AGA AAG GAG GTG ATC ga	17	1504 - 1518	> 100*
T.th. 15e	5`- AGA AAG GAG GTG ATC gga	18	1504 - 1518	80
T.th. 15f	5`- AGA AAG GAG GTG ATC ggg a	19	1504 - 1518	96
T.th. 15h	5`- agg ggg AGA AAG GAG GTG ATC	21	1504 - 1518	25
T.th. 15i	5`- AGA AAG GAG GTG ATC ggg gga	21	1504 - 1518	85
T.th. 15j	5`- ag ggg AGA AAG GAG GTG ATC ggg gga	25	1504 - 1518	> 100*
T.th. 15k	5`- a xxx AGA AAG GAG GTG ATC	19	1504 - 1518	72
T.th. 15l	5`- xxx AGA AAG GAG GTG ATC	18	1504 - 1518	54
T.th. 15m	5`- axx AGA AAG GAG GTG ATC	18	1504 - 1518	26
T.th. 15n	5`- AGA AAG GAG GTG ATC xxx a	19	1504 - 1518	35
T.th. 15o	5`- AGA AAG GAG GTG ATC xxa	18	1504 - 1518	21

x = 6-thio-dG

* binding > 100% means that more than 1 molecule of oligonucleotide binds per 30S subunit

Lowercase letters indicate that a tail, not complementary to 16S sequence, was added to the oligonucleotides

4.1.2 Crystallographic analysis of the 30S·TAMM·oligonucleotide complex

The 30S·TAMM·oligonucleotide complex was obtained incubating the 30S with an excess of TAMM labelled oligonuclotide and purified by sucrose cushion centrifugation (see section 3.4.8).
The crystallisation of the 30S·oligo complexes was not always successful probably because the rather unstable nature of the cDNA:RNA hybrids or because the oligonucleotide bound to the 30S interfered with contacts in the crystal network. Only for the complex 30S·oligo[T.th. 9c] very small crystals, that were not useful for X-ray analysis, were obtained.
Since the co-crystallisation did not yielded useful crystals the labelled oligonucleotides were then used for soaking of the T30S crystals (see section 3.7.2).
To check the influence of the oligonucleotide binding on the crystal properties, non-modified oligonucleotides were diffused into native T30S crystals. After soaking, some of these oligonucleotides had a marked effect on the resolution of the crystals. Some of them produced a decrease in resolution, probably because the regions where they bind are involved in the crystal network, and some of them did not change or even improved the resolution of the crystals, probably by stabilising regions exposed to the solvent.
The best resolution was achieved when a 19 base long oligonucleotide (T.th. 15k) complementary to the 3' end region of the 16S rRNA was used to soak the crystals. Crystals soaked in this modified oligonucleotide gave isomorphous derivatives and data were collected to 3.8 Å. Preliminary crystallographic analysis were performed leading to difference Patterson maps showing peaks which could account for the three TAMM molecules bound to the 19 nucleotide oligonucleotide. This allowed us to identify the 3' end of the 16S rRNA (Figure 9).
No data could be collected from crystals to which DNA oligonucleotides complementing the 16S rRNA around base 1400 (decoding centre) were diffused, since they introduced a resolution drop to 12-15 Å accompanied by a dramatic increase in the mosaic spread.

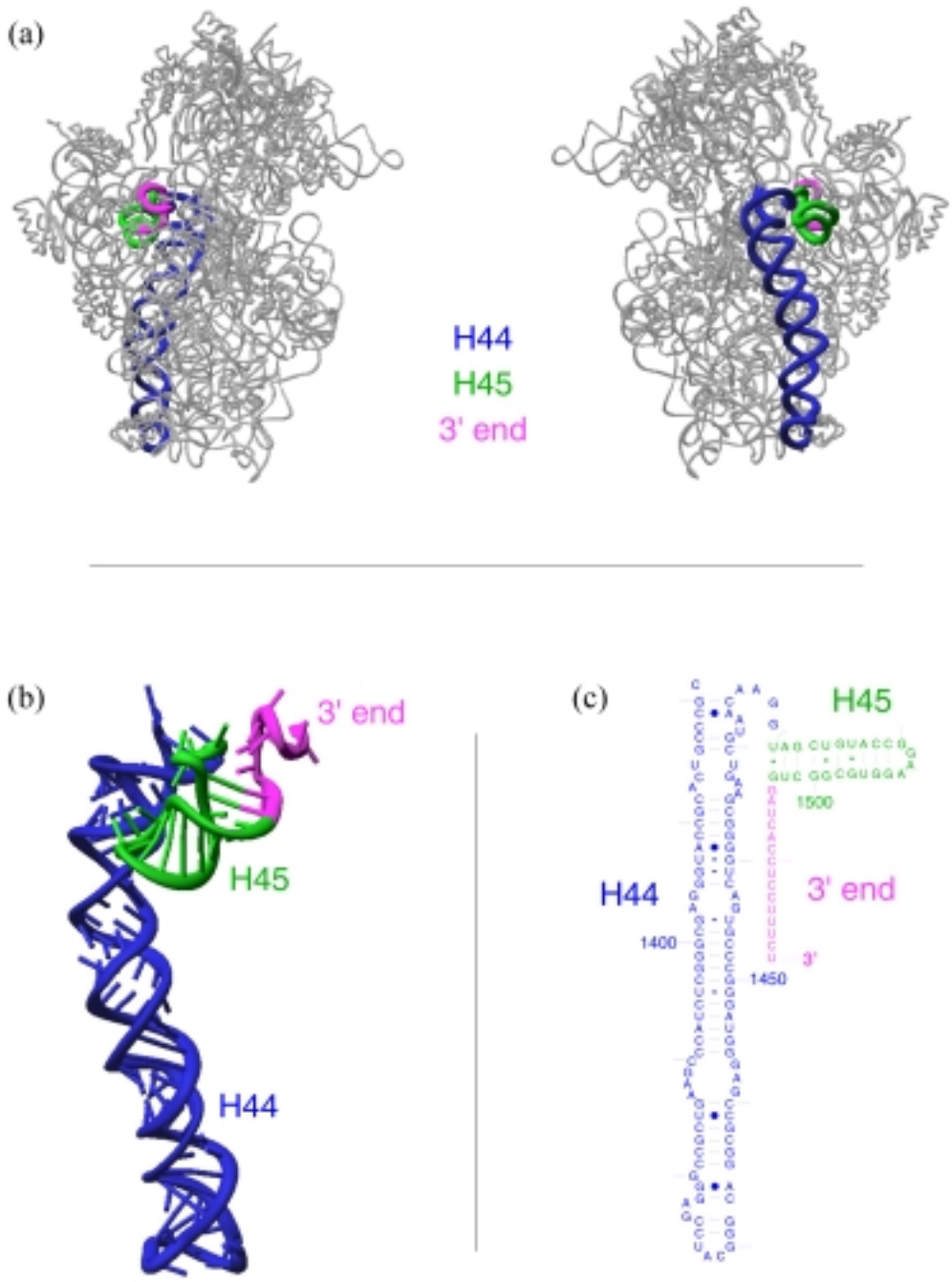

Figure 9. *Model of the 3' minor domain of the 16S rRNA from T. thermophilus.*
(a) Mono view of the 30S subunit evidencing the 3' terminal region (pink), helix 44 (blue) and helix 45 (green). The two images are rotated 180° one respect to the other. (b) Mono view of the 3' terminal region, helix 44 and helix 45. (c) Secondary structure prediction of the 3' terminal region, helix 44 and helix 45 (Gutell et al., 1999).

4.2 The initiation factor 3

The initiation factor 3 is an evolutionary conserved protein composed of two spatially separated domains (N-terminal and C-terminal) joined through a flexible linker. The structure of the two domains has been solved separately by NMR (Garcia et al., 1995a/b) and by crystallography (Biou et al., 1995). Figure 10a shows the sequence alignment of IF3 from several species.
In *Thermus thermophilus*, IF3 is a 172 amino-acids long protein having a predicted molecular weight of 19800 Da, with an isolectric point of 10.4.

We cloned, overproduced and purified the wild type form of *T. thermophilus* IF3, the C-terminal domain (IF3-C, amino acids 71-171) and a mutated form containing a cysteine tail on the N-terminal (IF3cys) (Figure 10b). We subsequently used them for crystallographic studies in their complexes with the 30S subunit.
The C-terminal domain was chosen because is the one carrying the residues involved in 30S binding (De Bellis et al., 1992; Ohsawa & Gualerzi, 1981) and is able to dissociate the 70S (Garcia et al., 1995), while the N-terminal domain is the one that has been proposed to be responsible for the proof-reading activity of IF3 (Bruhns & Gualerzi, 1980; De Bellis et al., 1992). An advantage in using the C-terminal domain is its size. The C-terminal domain is composed of 100 amino acids for a total molecular weight of around 12000 Da and therefore, suitable for soaking of the T30S crystals.
IF3 having a three-cysteine tail on the N-terminal end of the protein was cloned to bind heavy-atoms, in this case mercury, to IF3 for easier localisation by difference Fourier maps. The N-terminal end of IF3 was chosen to bind heavy atoms, because biochemical data showed that it is the less involved in ribosome binding (Sette et al., 1999). Thus, attachment of heavy atoms on this region of IF3 should not interfere with the binding of IF3 to the 30S. Introduction of cysteine residues inside the sequence was avoided because it could interfere with the binding of IF3 to the 30S subunit. The need to engineer the protein to introduce cysteine residues was due to the fact that thermophilic proteins are in general very poor in cysteines and this can be easily seen in the sequence alignment (Figure 10a). IF3 from *T. thermophilus* has no cysteine while IF3 from other bacteria species has at least one.

(a)

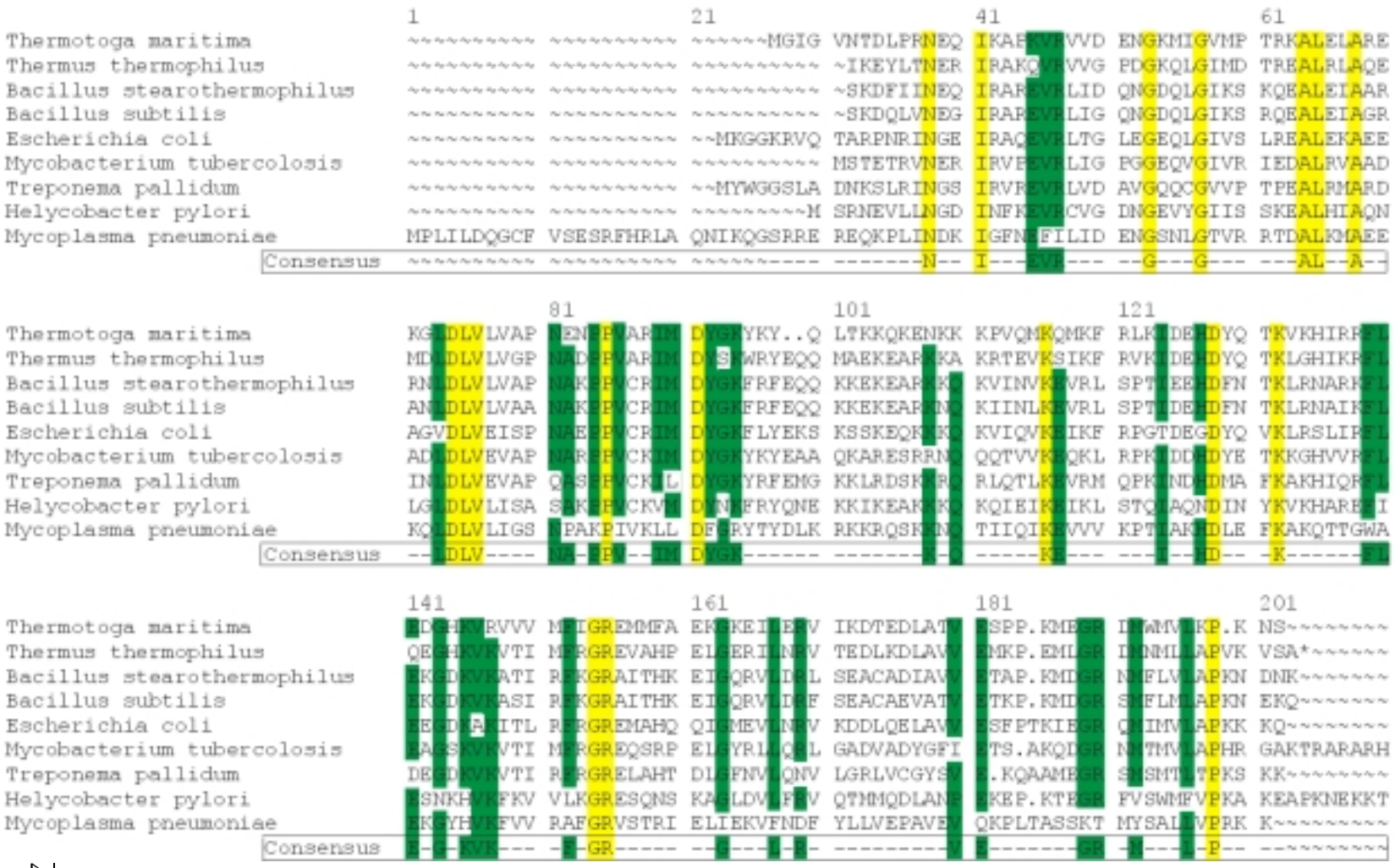
1
21
41
61
Thermotoga maritima
Thermus thermophilus
Bacillus stearothermophilus
Bacillus subtilis
Escherichia coli
Mycobacterium tuberculosis
Treponema pallidum
Helycobacter pylori
Mycoplasma pneumoniae
Consensus
81
101
121
141
161
181
201

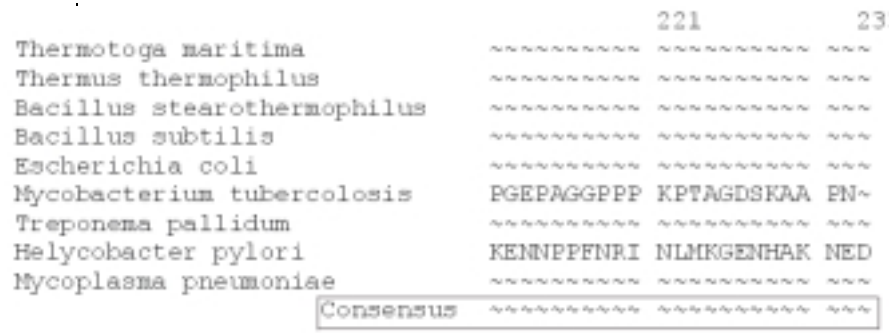

(b)

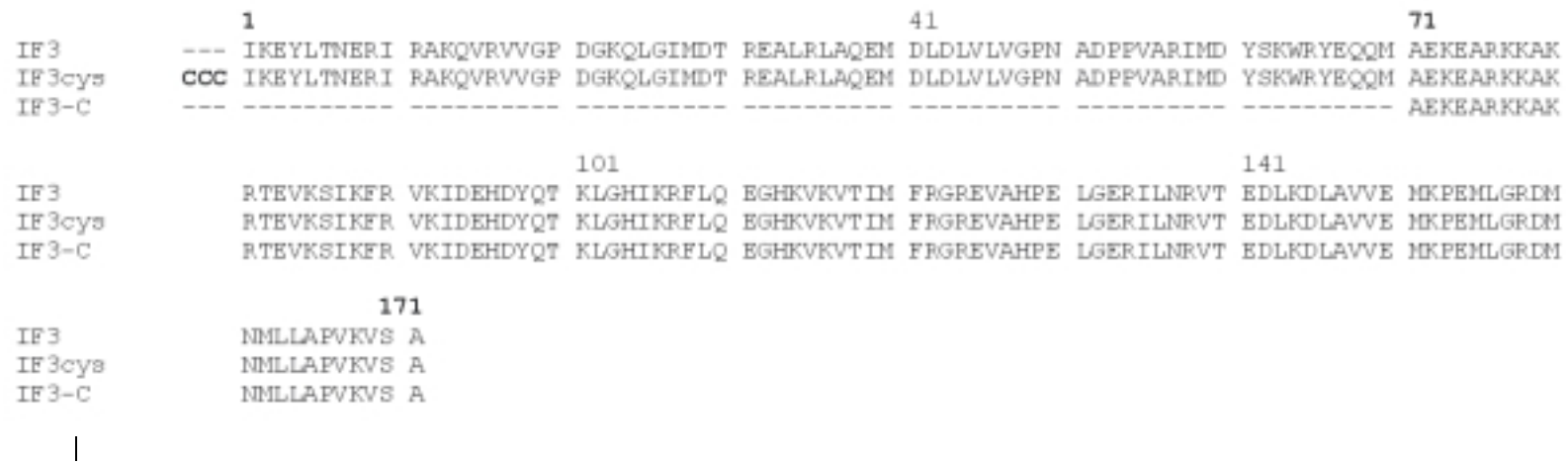

Figure 10. *Sequence alignment of IF3 from several species.*

a) Amino acids conserved in all nine species are enclosed in a yellow box. Amino acids conserved in at least seven out of nine

4.2.1 Different cloning strategies for *T. thermophilus* IF3, IF3-C and IF3cys

IF3: the gene *infC* coding for IF3 in *T. thermophilus* contains an internal BamHI site (position 401). Thus, this fact does not allow to simply amplifying the gene, digest the two ends with NdeI and BamHI and insert the fragment into the pET11a vector (Studier, 1990), but a different strategy had to be used.
For the cloning of IF3 the system based on two PCR amplifications with different primer pairs was used (Dunford and Dyer, 1997). This method is not affected by the presence within PCR products of restriction sites identical to those used for cloning since it does not require the digestion of the PCR product with restriction enzymes. The first primer pair comprised a forward primer specific for the target sequence with a 5' extension corresponding to the NdeI site and a reverse primer specific to the target sequence alone. The second pair contained forward and reverse primers with the same target-specific sequences as the first pair but with the reverse primer having a 5' extension having a BamHI site. Amplification products were mixed in equimolar amounts, heat denatured and re-annealed for 1 hour at room temperature. In this way, since the appropriate sites are given directly by the oligonucleotides, there is no need to cut the PCR products with restriction enzymes. After re-annealing, four different products can be formed. Only the duplexes formed by the association of single strands with the appropriate 5' extensions (25% of the annealed products) could be ligated with the vector digested with the corresponding restriction enzymes. The PCR was carried out using the high-fidelity thermostable *Pfu* DNA polymerase (Cline et al., 1996).
This method is successful with any restriction enzyme generating a defined 5' or 3' overhang. The use of high-fidelity thermostable DNA polymerases, which do not add additional nucleotides to the amplification products, should ensure the creation of the correct cohesive ends for ligation. The advantages of this method include the ability to define the ends of cloned fragments by careful primer design, resulting in the retention or ablation of restriction sites. This may be desirable for maintenance of reading frame and specific codons for correct protein expression or for subsequent cloning steps.
The following oligonucleotides were used:

		NdeI start codon
		↓ ↓
A) upper	5'- **CATatg** AAG GAG TAC CTG ACC AAC GAA CGC ATA CGC GCC AAA	
lower	5'- CAT CAG GCG GAG ACC TTC ACC GGG GCG AGG A	
B) upper	5'- TGA AGG AGT ACC TGA CCA ACG AAC GCA TAC GCG CCA AA	
lower	5'- **GGA TCC atc** AGG CGG AGA CCT TCA CCG GGG CGA GGA	
	↑ ↑	
	BamHI stop codon	

The restriction sites are marked in bold and the start and stop codons are marked in bold and lowercase. Nucleotides in grey represent the part of the restriction site not included in

the primers. The rare initiator codon of the *infC* gene (ATA) was modified here with the canonical ATG initiator codon, to improve the over-production of IF3.
The expression vector pET11a was digested with NdeI and BamHI and subsequently ligated to the re-annealed amplification products and transformed into *E. coli* XL1 Blue by electroporation. The plasmid DNA was recovered from the transformants using standard procedures (see section 3.2.3) and the presence of an insert having the correct size and the expected ends was confirmed by digestion with the appropriate (NdeI, BamHI) restriction enzymes.

IF3-C: the sequence of IF3 from amino acid 71 to amino acid 171 (IF3-C) was amplified using PCR in order to have the C-terminal domain. The plasmid containing the IF3 sequence (pET11a-IF3) was amplified using the following couple of primers:

```
                          NdeI      start codon
                          ↓   ↓
upper  5'- GGA ATT C**CAT atg** GCG GAG AAG GAG GCC CGG AAG
lower  5'- GA**AG atc** TTC CTA GGC GGA GAC CTT CAC C
             ↑   ↑
          BglII      stop codon
```

The restriction sites are marked in bold and the start and stop codons are marked in bold and lowercase. The PCR product was digested using BglII and NdeI and cloned in pET11a digested with BamHI and NdeI. The use of BglII instead of BamHI for the PCR product was necessary because BamHI cuts inside the IF3-C nucleotide sequence. BglII and BamHI give compatible ends, and recreate the BamHI restriction site. This is an alternative way to the method used for IF3 that also avoids the problem of the internal BamHI restriction site in the sequence.

IF3cys: for the cloning of IF3cys three PCR reaction were used and the cysteines were added in sequential PCR steps. It was not possible to do a single PCR step because it was found no oligonucleotides pair suitable for the amplification in order to add the three cysteines and the necessary restriction sites in one single step. The following oligonucleotides were used:

upper (1) 5'- **TGC TGC** ATA AAG GAG TAC CTG ACC AAC GAA
upper (2) 5'- C **CAT atg TGC TGC TGC** ATA AAG GAG TAC CTG A

```
                                    NdeI      start codon
                                    ↓   ↓
upper (3)  5'- CGG AAT TC**C CAT atg TGC TGC TGC** ATA AA
lower      5'- GA**AG atc** TTC CTA GGC GGA GAC CT
                  ↑   ↑
               BglII      stop codon
```

The restriction sites are marked in bold, the start and stop codon are marked in bold and lowercase and the cysteine codon are marked in bold and underlined. The PCR product was digested with BglII and NdeI (see IF3-C) and cloned into pET11a vector.

4.2.2 Optimisation of overproduction and purification of IF3, IF3-C and IF3cys

The vector containing the IF3 insert was transformed in *E. coli* BL21(DE3)pLys and the cells were grown in M9ZB medium in presence of ampicillin and choramphenicol (see section 3.5.1).
The parameters for the overexpression were optimised in a small volume culture. It was found that the highest amount of protein for all IF3 variants was obtained when the cultures were induced with 1 mM IPTG, once they had reached an absorbance of 0.7 (A_{560}). Similarly, it was found that three hours incubation at 37°C after induction was the optimum time to obtain the largest amount of over-produced IF3 variants. For IF3 the yield of pure protein was 15 mg/ml, for IF3-C was 5 mg/ml and for IF3cys was 12 mg/ml.

The purification procedure was first optimised for IF3 and then the same procedure was applied for IF3-C and IF3cys since the three IF3 variants have practically the same isoelectric point.
The cells were suspended in lysis buffer and disrupted using a French Press. The whole cell lysate was then heated for 30 min at 60°C (see section 3.5.4.1) and the supernatant containing IF3 loaded onto a DEAE-Sepharose column (see section 3.5.4.2). In the next purification step the fractions containing IF3 were loaded onto a Resource S column, FPLC (see section 3.5.4.2). IF3 was eluted at a NaCl concentration between 180 and 200 mM (Figure 11). The purity degree at this point was estimated by SDS-PAGE to be between 90 and 95%.

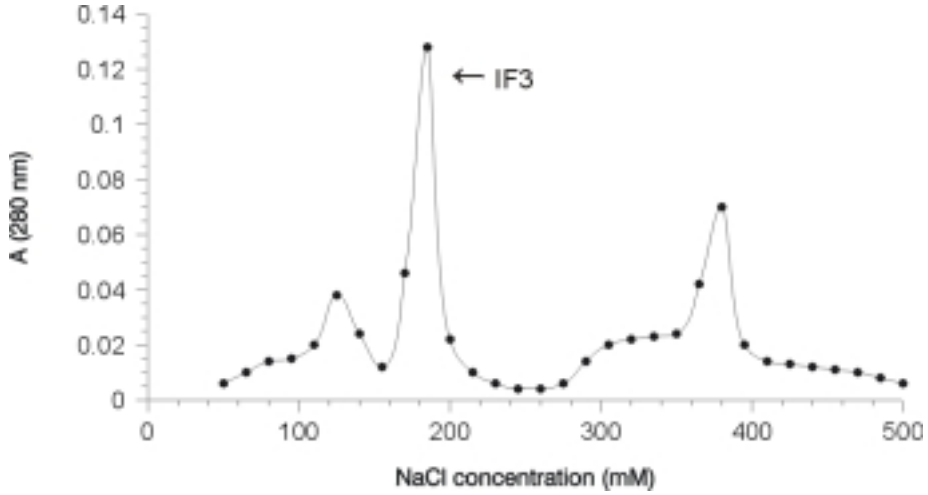

Figure 11. *Resource S-FPLC profile.*

T. thermophilus IF3 is eluted at a NaCl concentration of 185 mM.

Even though the protein was rather pure after the resource S column, it was further purified by hydrophobic chromatography (see section 4.5.4.3). After this last purification step the degree of purity was estimated from SDS-PAGE to be more than 97% (Figure 12).
Throughout the whole procedure protease inhibitors (PMSF, benzamidine) were added to prevent degradation of the protein.

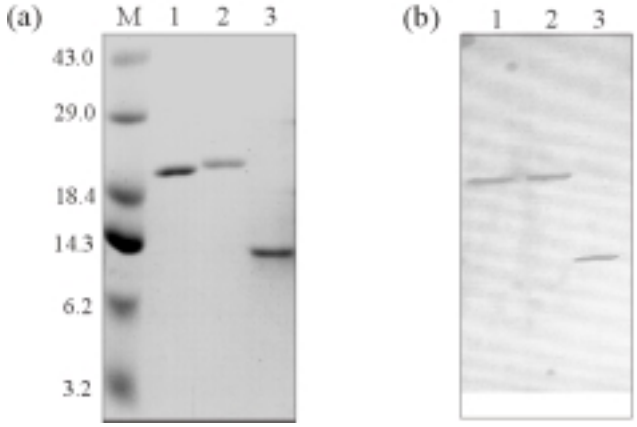

Figure 12. *SDS-PAGE and western-blot of pure IF3, IF3cys and IF3-C.*
(a) SDS-PAGE 15%. Lane M: molecular weight marker; lane 1: IF3; lane 2: IF3cys; lane 3: IF3-C. (b) Western-blot using anti-IF3 and IF3-C IgG respectively, of the gel shown in figure 12a.

The 70S dissociation activity of the purified IF3 variants was tested as described in section 3.5.8, by incubating the 70S ribosomes with ten-fold excess of IF3, IF3-C or IF3cys in a buffer containing 10 mM $MgCl_2$. At this Mg^{2+} concentration the *T. thermophilus* 70S does not dissociate in its two subunits as shown on the sucrose gradient centrifugation profile (Figure13a). The reaction mixtures containing 70S plus IF3 were loaded on a sucrose gradient and after centrifugation the gradient was fractionated and the absorbance of the fractions was monitored. Once IF3 is added the 70S dissociates completely in 30S and 50S (Figure13b). Similar results were obtained for IF3cys and IF3-C (data not shown).

The fractions from sucrose gradient centrifugation containing the 30S subunit were analysed by SDS and western blot. All the IF3 variants were found bound to the 30S subunit in stoichiometric amounts (Figure 14).
In contrast to IF3 and IF3cys that in a SDS-PAGE migrate in a region where no ribosomal proteins are detected, IF3-C co-migrates in the one dimensional SDS-PAGE together with some of the ribosomal proteins, making the unambiguous detection of its presence difficult. Therefore, the use of the western blot with polyclonal antibodies against IF3-C allowed unequivocal detection of the bound IF3-C to the T30S subunit.

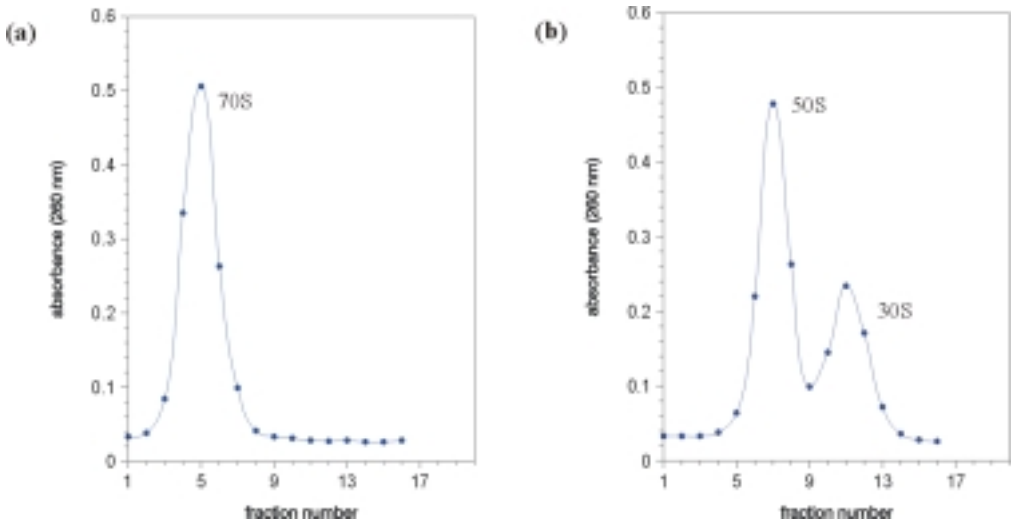

Figure 13. *Sucrose gradient sedimentation profiles of the T. thermophilus 70S in the presence and in the absence of IF3.*

(a) T70S in buffer containing 10 mM $MgCl_2$. (b) T70S incubated with a 10-fold molar excess of IF3 in buffer containing 10 mM $MgCl_2$.

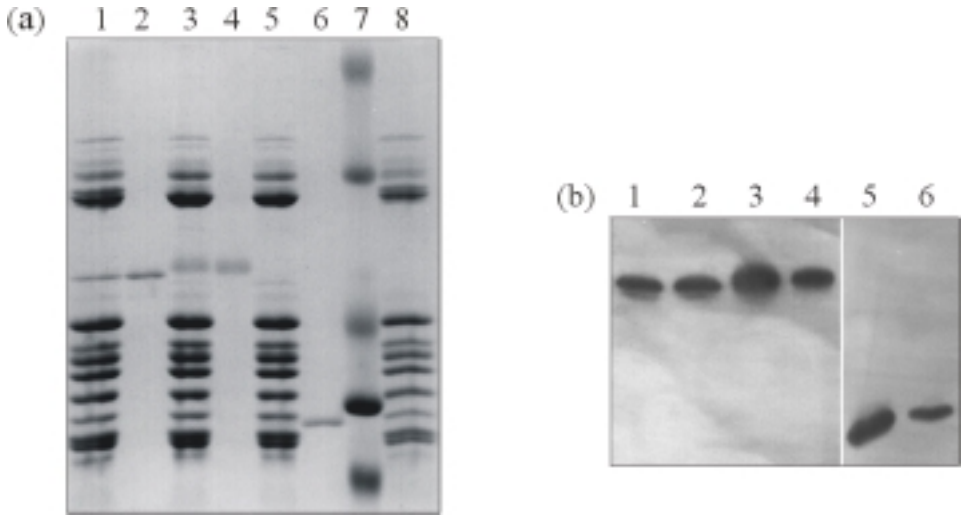

Figure 14. *SDS-PAGE and western-blot of 30S·IF3s complexes isolated from the 30S peak after sucrose gradient centrifugation.*

(a) SDS-PAGE 15%. Lane 1: 30S·IF3 (100 pmol); lane 2: pure IF3 (100 pmol); lane 3: 30S·IF3cys (100 pmol); lane 4: pure IF3cys(100 pmol); lane 5: 30S·IF3-C (100 pmol); lane 6: pure IF3-C (100 pmol); lane 7: molecular weight marker; lane 8: 30S control (72 pmol). (b) Western-blot of the gel from figure 14a.

4.2.3 Analysis of the 30S·IF3s complexes

30S·IF3, 30S·IF3-C and 30S·IF3cys: the 30S·IF3s complexes were formed incubating the 30S subunit with an excess of IF3 (see section 3.5.9). The complexes were purified as described in section 3.5.9 and analysed by SDS-PAGE. We found that IF3 was bound to the 30S subunit in a stochiometric amount. The affinity of IF3 for the 30S subunit is reported in literature to be around 10^7 M^{-1} (Weiel & Hershey, 1981) and we found that the complexes are stable after sucrose cushion or zonal centrifugation.
The purification of the complex and the choice of the buffer in which to keep it, were crucial for crystallising the sample. The use of sucrose cushion centrifugation (see section 3.3.5) was a useful technique to obtain the pure 30S·IF3 complex starting from amounts between 15 and 200 OD, with a yield between 70 and 90% of the starting amount.

30S·IF3cys·TAMM: the over-expressed IF3cys was labelled with TAMM. In the same manner as for the cDNA (see section 4.1.1) three of the four mercury atoms of the TAMM molecules were blocked incubating the TAMM with a three molar excess of [^{35}S]cysteine. The IF3cys·TAMM complex was purified by gel filtration. To determine the percentage of binding of [^{35}S]Cys·TAMM to IF3cys, the absorbance at 280 nm and radioactivity were monitored. The binding was also checked by SDS-PAGE. The samples were loaded using sample loading buffer without β-mercapthoethanol and were not heated at 95°C to avoid the dissociation of [^{35}S]Cys·TAMM from the complex. The gel was stained, destained, dried and exposed in a phosphor imager cassette. The gel was scanned (Molecular Dynamics, Image Quant) and as shown in the Figure 15 the radioactivity co-migrated together with IF3cys.
Furthermore, the activity of the IF3cys·TAMM was checked in the same way used for the native protein (see section 3.5.8). This control was performed because the crystals are obtained from 30S ribosomal subunits that have been incubated with IF3. Therefore it was necessary to know if the IF3cys·TAMM was still able to dissociate the 70S ribosome or if the binding of TAMM influenced somehow the activity of IF3. We found that the 70S could be dissociates by IF3cys·TAMM in the same way as by the native IF3, showing a dissociation profile similar to the one shown in Figure 13.
The complex IF3cys·TAMM was then used for labelling the 30S subunit. A three times excess of IF3cys·TAMM was incubated with 30S subunit for 30 min at 40°C. From this mixture 1-2 OD were loaded on a sucrose gradient 5-20% (w/v) and centrifuged. The gradient was fractionated and the absorbance at 260 nm and the radioactivity of each fraction monitored. The fractions containing the 30S subunit were loaded on a SDS-PAGE and the gel was analysed in the same way used for the IF3cys·TAMM complex. It was found that the radioactivity co-migrates with the 30S subunit in the sucrose gradient. Moreover, when the 30S obtained from the sucrose gradient was analysed by SDS-PAGE, we found that the radioactivity co-migrate with the IF3cys·TAMM band (Figure 15). We could therefore conclude that the IF3cys·TAMM complex binds to the 30S subunit and that its binding is stable enough to withstand a sucrose gradient centrifugation.
The absence of β-mercaptoethanol in the sample loading buffer used for the gel allows IF3cys to dimerise as shown in Figure 15. Anyway, in the 30S·IF3cys·TAMM complex, only IF3cys binds.

From the radioactivity that migrates together with the 30S subunit we could estimate the percentage of IF3cys·TAMM bound to the 30S subunit to be at least 70%. As for the oligonucleotides (see section 4.1.1) this calculation is statistical giving us therefore only a minimum binding.

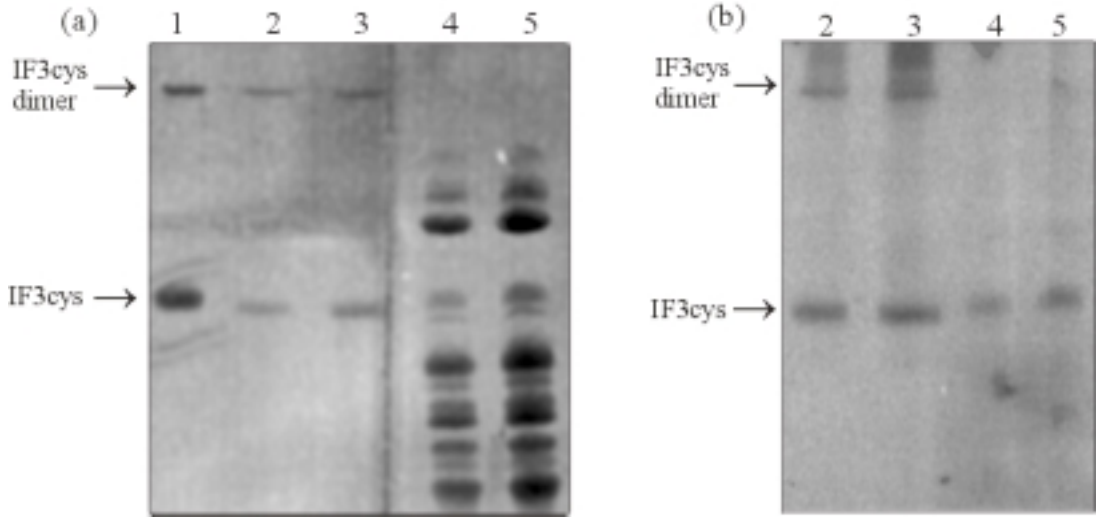

Figure 15. *Native PAGE and Phosphor Image of IF3cys·TAMM and of 30S·IF3cys·TAMM complexes. (a) Native PAGE. Lane 1: IF3cys (500 pmol); lane 2: IF3cys labelled with TAMM·[^{35}S]Cys (100 pmol); lane 3: IF3cys labelled with TAMM·[^{35}S]Cys (150 pmol); lane 4: 30S labelled with IF3cys·TAMM·[^{35}S]Cys (150 poml) from sucrose gradient centrifugation; lane 5: 30S labelled with IF3cys·TAMM·[^{35}S]Cys (300 pmol) from sucrose gradient centrifugation. (b) Phosphor Image of the radioactive gel of figure 15a. The radioactivity migrates together with the protein showing that IF3cys is labelled with TAMM·[^{35}S]Cys and that after incubation and sucrose cushion centrifugation the 30S is labelled with IF3cys·TAMM·[^{35}S]Cys.*

30S·IF3cys·$HgCl_2$: $HgCl_2$ was used as an alternative method to label IF3cys in the 30S·IF3 complex. IF3cys was labelled with mercury before binding to the 30S subunit. A five fold excess of protein was incubated with the 30S subunit and then with four fold excess of $HgCl_2$ at room temperature. The mix was then loaded on a sucrose cushion to separate by centrifugation the excess of IF3cys and $HgCl_2$ that were not bound to the 30S. Since TAMM, which is in molecular weight around five times bigger than $HgCl_2$ could bind to IF3cys without causing lost in the activity of the protein, and the IF3cys·TAMM complex could bind to the 30S subunit, we assumed that $HgCl_2$ could bind in the same way as TAMM.

4.2.4 Crystallisation and crystallographic analysis of the 30S·IF3s complexes

Crystallisation experiments were performed for 30S·IF3, 30S·IF3-C and 30S·IF3cys (with and without $HgCl_2$ or TAMM) complexes. IF3 is a relatively small protein (172 amino acids) when compared with the 30S ribosomal subunit, therefore we tried the same conditions for crystallisation used for the 30S alone (see section 3.7.1) but using the different 30S·IF3s complex instead.
In general crystals of 30S alone appears already in 4-8 days. The crystals of the 30S·IF3 complex appeared in 3-4 weeks together with precipitate, while the crystals of the 30S·IF3-C, 30S·IF3cys and 30S·IF3cys·Hg complexes appeared in 10-15 days.
Under the microscope the crystals of 30S and the different 30S·IF3s complexes were indistinguishable (Figure 16). Moreover, X-ray analysis of the 30S·IF3 crystals show that they belong to the same space group than the 30S subunit alone (see section 3.7.1).

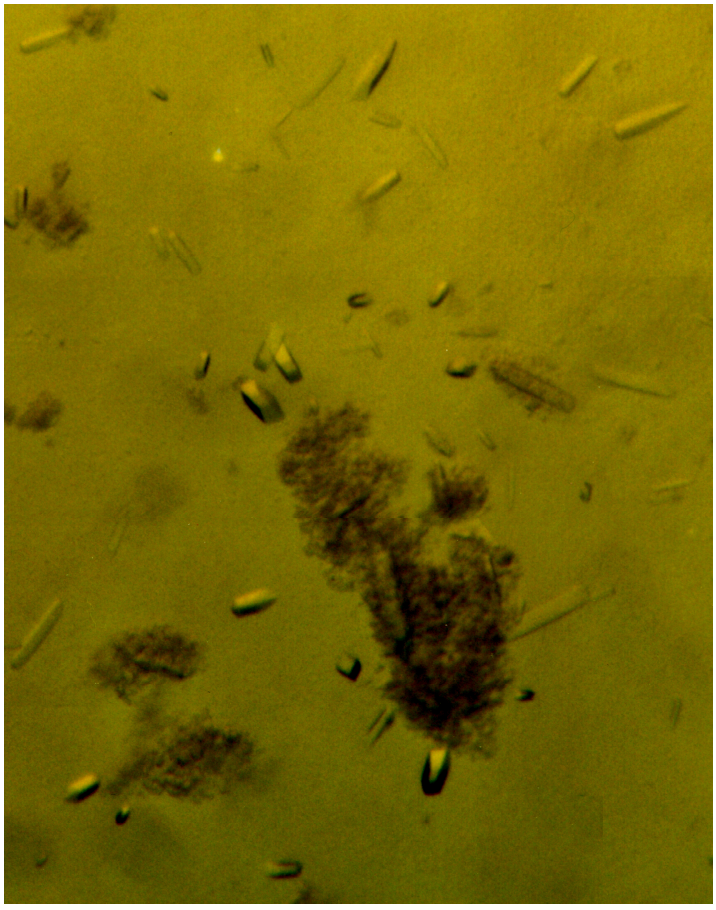

Figure 16. *Crystals of the 30S·IF3 complex.*
The crystals grew in 3 weeks at 20°C, using 1% MPD in the drop and 14% MPD in the reservoir. The size of the crystals of the 30S·IF3 complexes was between 120x40x40 and 300x60x60 µm.

To determine the presence of IF3, IF3-C and IF3cys in the crystals, around 50-100 crystals were transferred to a vessel filled with the stabilisation solution, which contains a higher percentage of MPD than the one used for crystallisation, and washed. The washing procedure was performed transferring the crystals from one vessel containing 500 µl of stabilisation solution to another containing the same amount of stabilisation solution. The procedure was repeated three times, then the crystals were transferred to a small tube, centrifuged shortly and the supernatant was removed. The pellet containing the washed crystals was suspended in SDS sample loading buffer and analysed by PAGE. For IF3-C a western-blot was necessary. As shown in Figure 17 the bands corresponding to IF3s are clearly visible indicating that the crystals of the 30S·IF3 complex do not loose IF3 during the crystallisation process. The binding was in stoichiometric amount.

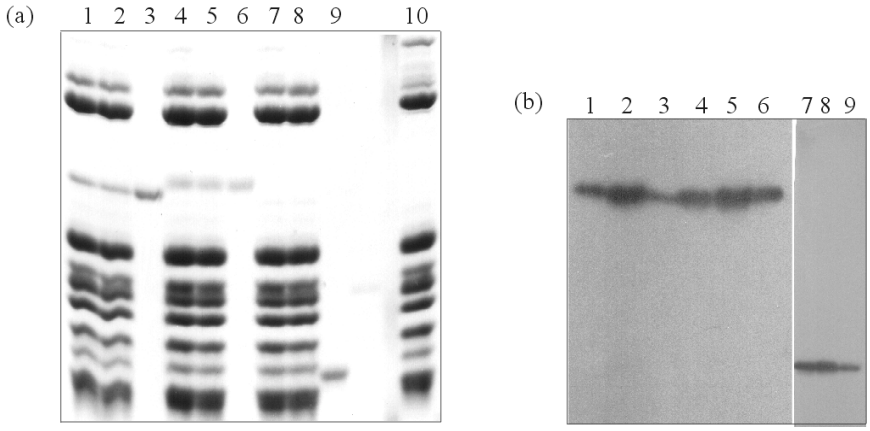

Figure 17. *SDS-PAGE and western-blot of the 30S·IF3s complexes used for crystallisation.*
(a) SDS-PAGE 15%. Lane 1: 30S·IF3 before crystallisation (100 pmol); lane 2: dissolved crystals of 30S·IF3 (100 pmol); lane 3: pure IF3 (100 pmol); lane 4: 30S·IF3cys before crystallisation (100 pmol); lane 5: dissolved crystals of 30S·IF3cys (100 pmol); lane 6: pure IF3cys (100 pmol); lane 7: 30S·IF3-C before crystallisation (100 pmol); lane 8: dissolved crystals of 30S·IF3-C (100 pmol); lane 9: pure IF3-C (100 pmol); lane 10: 30S subunit alone (100 pmol). (b) Western blot of the gel from figure 17a.

As an alternative process, IF3 and IF3-C were used for soaking of the 30S crystals. The soaking was performed as described in section 3.7.2. The crystals did not show any cracks under the microscope after the soaking procedure and, therefore, were used for X-ray analysis. The resolution of the IF3 soaked crystals was around 10 Å and no data were collected. For the IF3-C soaked crystals data were collect between 4 and 6 Å (Table 2).

Table 2. Results of crystallisation experiments of the 30S·IF3s complexes.

Complex	Crystals	Data collection	Resolution
30S·IF3	yes	yes	4 - 4.5 Å
30S·IF3cys	yes	no*	> 7 Å
30S·IF3-C	yes	no*	> 7 Å
30S·IF3cys·Hg	yes	no*	> 7 Å
30S·IF3cys·TAMM	no	----	----
30S (IF3 soaking)	----	no*	> 7 Å
30S (IF3-C soaking)	----	yes	4 - 4.5 Å

* Data was not collected due to the low resolution of the crystals.

4.3 Structure determination

The T30S subunit model described by Schlünzen et al., 2000 was used to determine the structures of three functionally relevant complexes: 30S·IF3-C, 30S·tetracycline and 30S·edeine. These were obtained by soaking crystals of the 30S subunit of *Thermus thermophilus* in solutions containing tetracycline, edeine or IF3C. The sigmaA weighted difference maps, calculated after refinement of the native structure against the observed structure factor amplitudes for each of the three complexes, confirmed the locations obtained from the difference Fourier between native and ligand data sets. Minor changes in the unit cell dimensions were observed for the soaked crystals. The results of the refinement of the structures of the 30S complexes including the ligands are shown in Table 3.
The resolution of the structures presented here limits our ability to deduce the exact chemical nature of the 30S/ligand interactions. In all cases, however, the electron density maps allowed unambiguous interpretations.
In this section, if not differently specified, bases of the 16S rRNA are numbered according to the *E. coli* sequence and helices are numbered as described by Mueller and Brimacombe, 1997.

4.3.1 Localisation of IF3-C in the 30S structure

The crystallographic data collected for the 30S crystals soaked into IF3-C allowed us to localise the C-terminal domain of IF3 and to dock the N-terminal domain IF3-N and the linker.

Table 3. Crystallographic statistics of data collection and refinement. Numbers in brackets describe the highest resolution bin.

Compound	Resolution [Å]	Unit Cell dimensions [Å]	Number Observed	Unique Reflections	Completeness [%]	<I>/<s(i)>	Rsym [%]	R/Rfree [%]
Native	40-3.2	a=b=407.0, c=176.0	2485385	228166	86.8 (83.2)	19.8 (2.0)	13.6 (38.1)	20.3/24.5
Tetracycline	35-4.5	a=b=406.9, c=175.2	365437	79036	89.7 (79.8)	9.1 (3.4)	9.9 (31.0)	22.3/25.4
Edeine	35-4.5	a=b=407.1, c=174.1	268539	66468	76.1 (68.2)	9.8 (2.5)	8.8 (41.8)	23.7/24.4
IF3C	35-4.2	a=b=407.5, c=174.8	417631	83090	81.5 (69.6)	9.2 (2.4)	9.9 (35.7)	20.5/26.4

The data collected for the crystals of the 30S·IF3 complex did not give the expected results. It was not possible to localise the IF3 even if the resolution was approximately the same as the one obtained for the T30S crystals soaked in IF3-C. One explanation can be the soaking with W18 (see section 3.7.2). W18 can compete with the whole IF3 for binding to the 30S and could displace IF3. We tried to collect data from the 30S·IF3 crystals not soaked in W18, but the resolution dropped to 7Å.

After refinement of the structure using the data of the 30S·IF3-C complex, the difference Fourier map revealed density that allowed the unambiguous accommodation of the two alpha-helices of IF3-C, whereas the beta-sheets and some side-chains of IF3-C were less well resolved. Neither the difference map nor the refinement of the complex indicated a significant conformational change in the 30S subunit upon IF3-C binding.
In our map IF3-C lies at the upper end of the platform on the solvent side (Figure 18a). It is located between H23, H26, and the 3' end of H45. In this location it would not physically block the interactions between the small and the large subunits. The contacts of IF3-C with the 16S RNA involve the bulge of H23 (719-723), H26 (833-839) and the 3' proximal end of H45 (1532-1534) close to the anti-Shine-Dalgarno (anti-SD) sequence. Additional contacts with the 30S subunit involve S2, S7, S11, and S18 (Figure 18b) Our results are consistent with those of cross-links of IF3 to 1506-1529 and 819-859 (Ehresmann et al., 1986), and crosslinks to proteins S7, S11 and S18 (MacKeen et al., 1980).
Residues 21-31 in the flexible N-terminal end of S2 are in contact with the loop connecting B6 and α-H4 of IF3-C. S7 interacts with IF3-C through its long C-terminal tail. This flexible part of S7 is partially organised in our structure by the heavy-atom (W18) that was used by us for phasing (Tocilj et al., 1999). Thus, it is possible that W18 interferes with the interactions between S7 and IF3-C. Residues 87-96 of S11 interact mainly with B5 of IF3-C. The contact area between S18 and IF3-C is rather large. Residues 7-18 of the N-terminal end of S18 wrap around IF3-C and face its inner beta-sheets, these S18 residues interact with the IF3-C residues 104-125 and 134-141 (*T. thermophilus* sequence). An additional contact is formed by residues 52-55 of S18 interacting with the loop between B5 and α-H3 of IF3-C. We found that the conformation of the N-terminal end of S18 depends on the soaking conditions of W18, indicating that this end of S18 is particularly flexible. Similarly, the N-terminal end of S2 and the C-terminal ends of S7 and S11 show different conformations in the two independently determined 30S structures (Schlünzen et al., 2000; Wimberly et al., 2000), indicating that these protein extensions are rather flexible. Thus, these protein extensions appear to act as tentacles, which enhance the binding and the placement of ribosomal factors like IF3.
NMR and mutagenesis studies of IF3 showed that in *E. coli* residues 99-116, 127-137, 145-155, and 168 are involved in IF3 binding to the 30S subunit (Sette et al., 1999). It was suggested that residues 99, 112, and 116 are the major RNA-binding residues, whereas 131-137 are the residues involved in IF3-C protein contacts (Sette et al., 1999). The results of these studies are consistent with the interactions that we observed by analysing the structure of the 30S·IF3-C complex (Figure 18b).

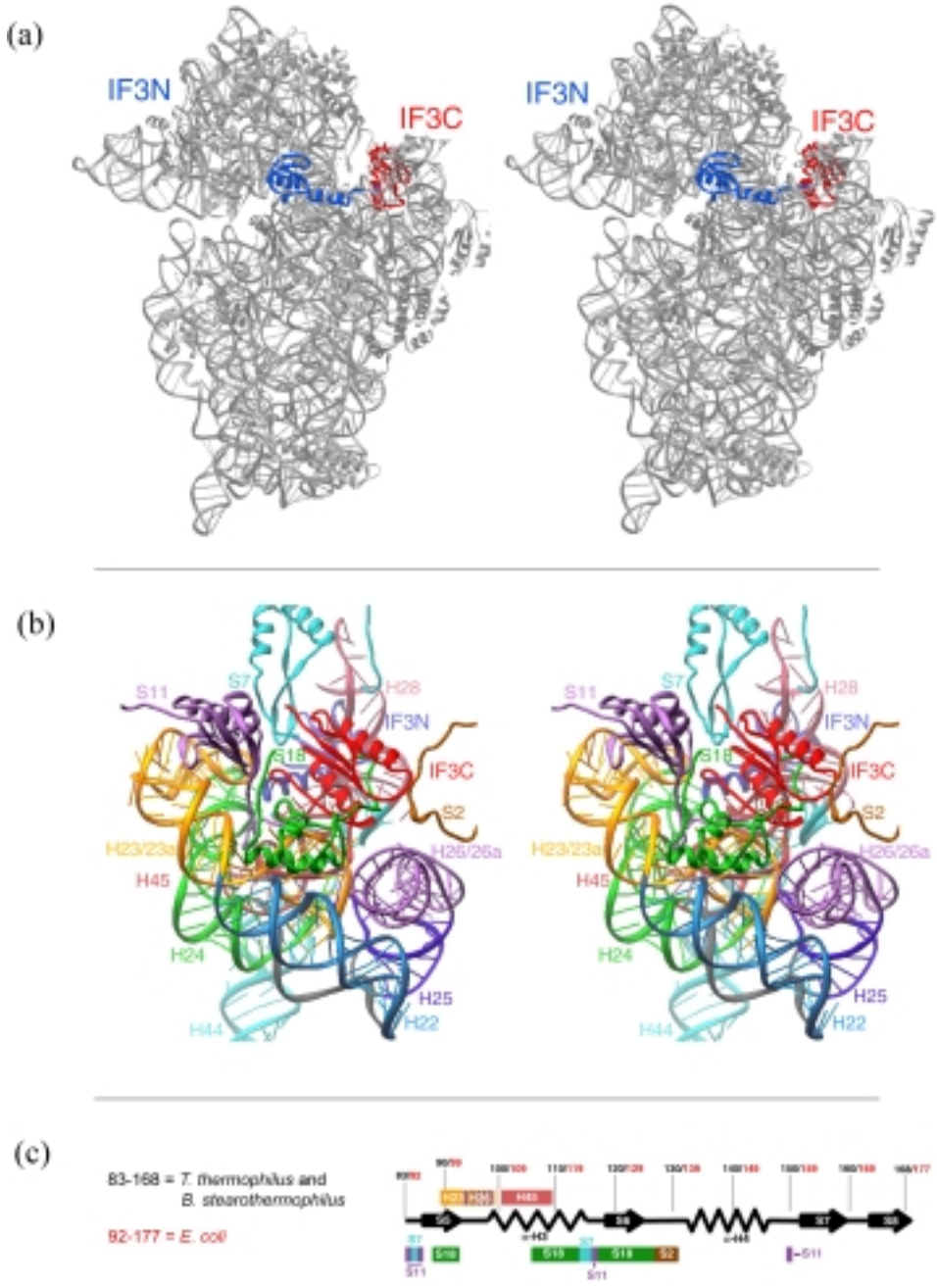

Figure 18. *Binding of IF3 to the small subunit.*

(a) The model of the complete 30S·IF3-C complex (IF3-C in red) and the docking of IF3-N (blue) are shown. (b) Stereo view of the model of the 30S·IF3 complex in the vicinity of IF3C. Parts of the 30S structure not involved in the interactions with IF3 are omitted for clarity. (c) Secondary structure of IF3-C (nomenclature Biou et al., 1995). Residues of IF3-C interacting with different RNA helices and ribosomal proteins are highlighted.

We attempted the docking of IF3-N to the 30S subunit so that its proposed function, the constraints posed by the position of IF3-C, and the existing biochemical data, were all satisfied. Docking was performed manually as well as with MOLFIT (Eisenstein et al., 1997) and the only location on the 30S subunit that could fulfil all these requirements was found in close proximity to the P-site (Figure18a). In this position IF3-N interacts with H28, H29, H31, H34, and H44 (via nucleotides 924-927 and 1381-1387 of H28, 1341 of H29, 966-968 of H31, 1062-1064 of H34, and 1398-1400 of H44). IF3-N hence contacts all helices known to be involved in the peptidyl-tRNA binding and could affect the RNA crosslinks C967xC1400 and C1402xC1501, as reported (Shapkina et al., 2000).
The binding of IF3-N leaves only a limited space for P-site tRNA, and requires small conformational changes for simultaneous binding of both IF3-N and P-site tRNA. This could shed light on the mechanism of IF3-N-mediated discrimination of non-canonical initiation codons or codon-anticodon complementarity. Docking the P-site tRNA into this model (Cate et al., 1999) shows close contacts between tRNA residues 31-35 and the N-terminal end of IF3-N, which could also explain the effect of IF3-N on the P-site tRNA crosslinks (Shapkina et al., 2000).

4.3.2 Localisation of tetracycline and edeine in the 30S structure

Two different antibiotics, edeine and tetracycline, have been used in this study. Edeine blocks the initiation process and tetracycline blocks the A-site tRNA binding. The two 30S·antibiotic complexes were obtained by soaking (see section 3.7.2) the 30S crystals into a 5 µM edeine solution and into a 4 µM tetracycline solution, respectively.
In table 4 are summarised the crystallographic sites found for edeine and tetracycline and the corresponding biochemical data. Figure 19 shows the binding sites determined for edeine and tetracycline. The results of the refinement of the structures of the 30S complexes including the ligands are summarised in table 3.

Table 4. **The crystallographically determined binding sites of tetracycline and edeine to the 30S ribosomal subunit, and the corresponding biochemical data.**

Ligand	RelativeOccup.*	Location in the 30S structure	Biochemical Data, less than 10Å distance
Edeine	1.0	A790-A792(H24), G926 (H28), U1498, U1505 (H45) G693xC795[#] (H23xH24)	Protection against chemical modification of G693, A794, C795, G926. Weak protection of A790, G791, A1394 (Moazed and Noller, 1987)
Tet-1	1.0	A964-G966 (H31), G1053, C1054 (H34), A1196-G1198 (H34)	Enhanced reactivity of U1052 and U1054 (Moazed and Noller, 1987) Tetracycline resistant G1058C Mutation (Ross et al., 1998) Inhibits crosslink of C967xC1400 (Noah et al., 1999)
Tet-2	0.7	Lys85, Val92-Leu96 and Leu188 (S4)	---
Tet-3	0.65	C1162-G1164 (H40), G1172-G1174 (H40)	---
Tet-4	0.53	G941,G942 (H29), C1342, G1343 (H29), A1349-U1351 (H43), Gln124 (S9)	Crosslinked to G1338 (Oehler et al., 1997)
Tet-5	0.41	U244-G247 (H11), G894-G896 (H27)	Protection against chemical modification of A892 (Moazed and Noller, 1987) Decreases the crosslink U244xG894 (Noah et al., 1999) Crosslinked to G890 (Oehler et al., 1997)
Tet-6	0.41	A937-A938 (H28/H29), C1378-U1380 (H28), Arg4, Arg5 (S7), Arg120 (S9)	Photochemical crosslink: S7 (Goldman et al., 1983) Inhibits the crosslink of 967xC1400 (Noah et al., 1999)

[#]Corresponds to the edeine induced cross-helix base pair.
*Relative occupancies are defined as fractions of the Tet-1 occupancy.

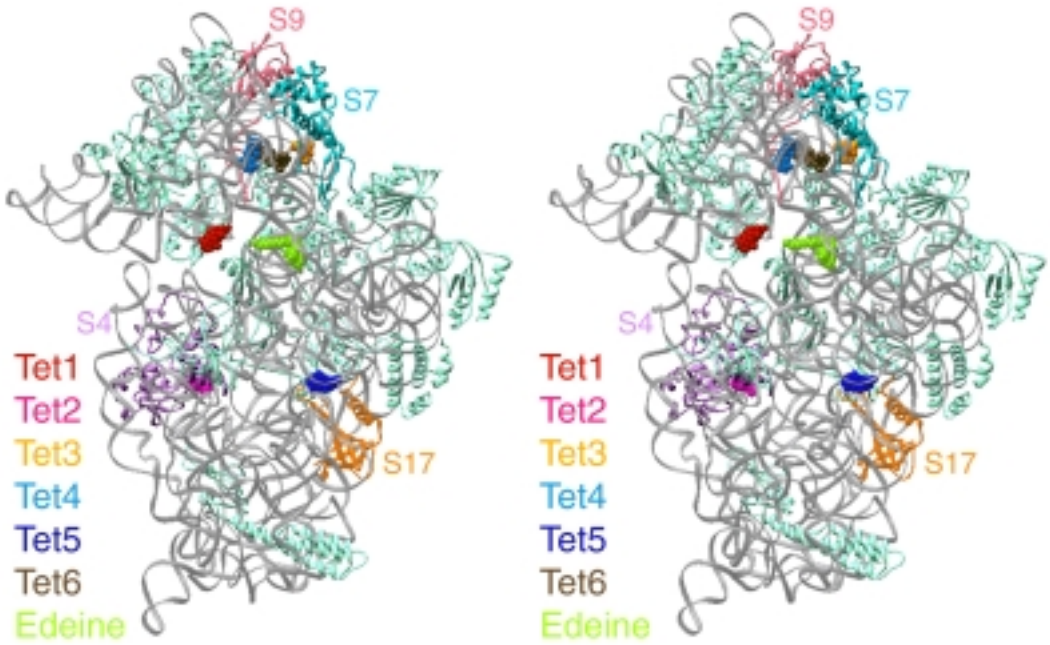

Figure 19. *Binding site of edeine and tetracycline to the 30S subunit.*

The binding sites of tetracycline and edeine are indicated in the stereo view of the 3.2 Å structure of the 30S ribosomal subunit. Ribosomal proteins interacting with tetracycline have been coloured and labelled.

Edeine. The complex of the 30S subunit with edeine revealed two strong peaks in the difference density maps, accounting for the binding site of edeine and the formation of a new RNA base pair. Edeine was located in the vicinity of the E-site, interacting with H24, H28, H44 and H45, and connecting universally conserved bases involved in the initiation process (Figure 19, Figure 20a and Table 4). Docking the peptidyl-tRNA at the P-site of the 30S structure shows that the spermidine-like moiety of edeine interacts with the backbone of the tRNA. The interactions of edeine with the P-site tRNA could therefore explain the reduction of the affinity of the peptidyl-tRNA for the P-site.

The beta-tyrosine part of edeine interacts with G926 in a way that mimics a regular RNA base pair. The position of edeine is further stabilised through its interactions with the backbone of the penultimate helix (H44), namely U1498, and G1505 in H45. RNA residues 790-792 in the loop of H24 interact mainly through their sugars with the hydrophobic side of edeine. These interactions result in a small distortion of H24, which is sufficient to induce a cross-helix base pairing between C795 in the loop of H24 and G693 in the loop of H23. The formation of this base pair might lead to an undesirable stabilisation of the conformation of the platform, and in this way contribute to the inhibitory activity of edeine.

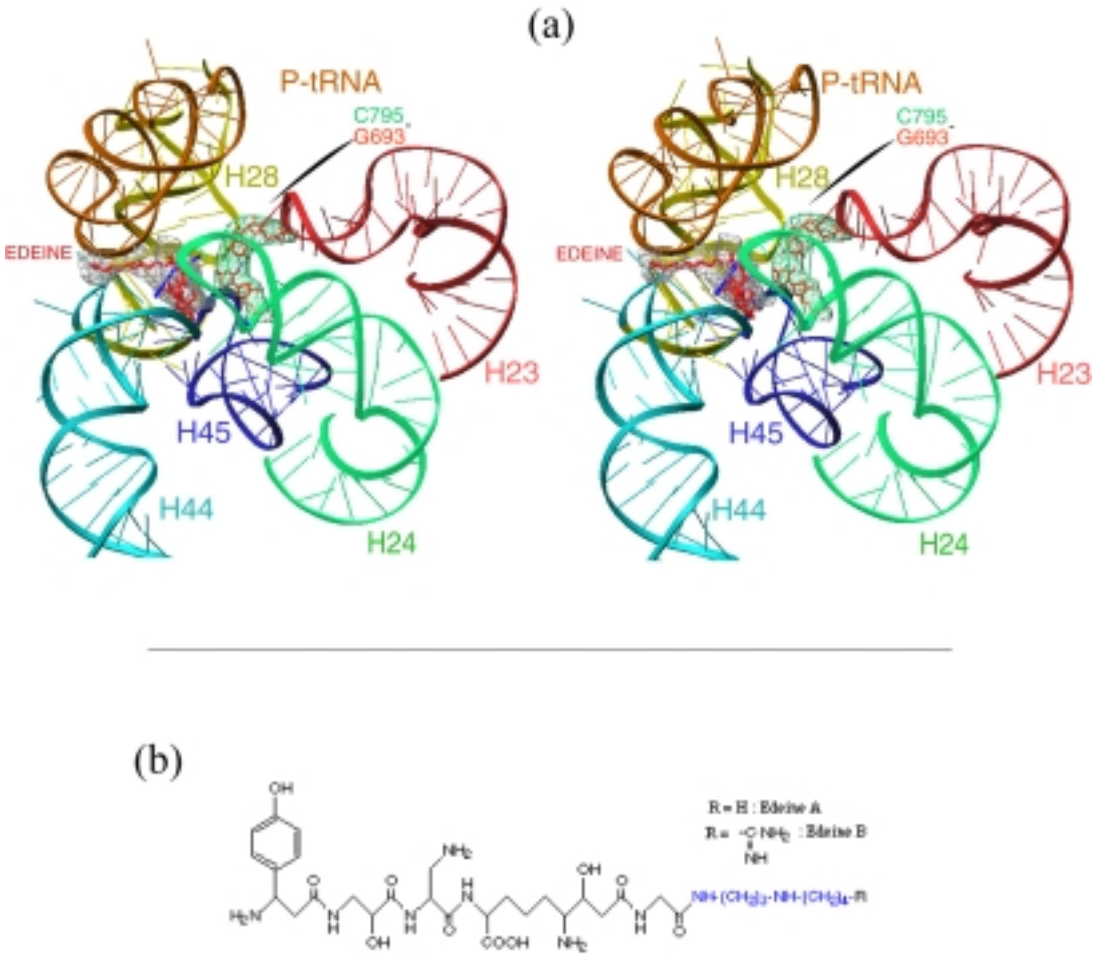

Figure 20. *Details of the binding sites of edeine.*

(a) Stereo view of the binding site of edeine. The image shows the sigmaA weighted difference density at contour levels of 3.2 sigma for both edeine and the RNA base pair induced upon its binding. (b) Chemical structure of edeine.

Tetracycline. We identified six tetracycline-binding sites (Tet-1 to Tet-6) on the 30S subunit (Figure 19), with relative occupancies ranging from 1 to 0.41 (Table 4, Figure 21). Tet-1, the site with the highest occupancy, is located between the distorted minor groove of H34 and the stem loop of H31, near to the A site where the aminoacyl-tRNA (Cate et al., 1999) was docked onto the 30S structure (Schlünzen et al., 2000). The five additional tetracycline sites are found at various locations in the head and the upper half of the body. The observation of multiple tetracycline binding sites was not unexpected, since several binding sites for tetracycline had already been suggested by biochemical experiments (Table 4).

The Tet-1 binding site is located in a pocket formed by residues 1054-1056 and 1196-1200 of H34, and 964-967 of H31 (Figure 21a). Bases 1196 and 1054, which are pointing out of H34 towards the A-site, form a clamp that holds the tetracycline molecule by hydrophobic interactions. Upon binding, the gap between these two bases becomes slightly wider. Aside from this local conformational change we did not observe any significant changes of the 30S subunit. This finding is consistent with toeprinting experiments in the presence of tetracycline (Jerinic and Joseph, 2000). Tet-1 interacts with the sugar-phosphate backbone of H34. This interaction seems to be co-ordinated through a magnesium ion, in a fashion similar to the interaction between the Mg-tetracycline complex and the tetracycline repressor tet(R) (Orth et al., 1999).

Tet-2 is located in a hydrophobic pocket of S4 (Figure 21b) and is the only tetracycline-binding site not involved in interactions with the 16S rRNA. This pocket is formed by a helix-loop-helix motif (residues 78-98 and residues 185-192). Arginine 187 and lysine 85, which are not involved in RNA or protein-protein interaction, close the pocket on the hydrophilic side of tetracycline. Tet-3 is buried inside H40, between its stem loop and its tetraloop (Figure 21c). The tetracycline interacts with U1159 of H40, which points back towards the tetraloop of H40, and the RNA residues adjacent to the tetraloop (1146/47 and 1153/54).

Tet-4 is located in a cavity formed by H29, H30, and H43 (Figure 21d). It interacts with the bases of the RNA residues 941-943 of H29 and those of the RNA residues 1342/43 of H43. Furthermore, it interacts with the RNA backbone of residues 1349/50 of H43 and G1233 of H30. Gln124 at the C-terminal end of S9 closes the cavity between H30 and H43. Tet-5 lies in a rather tight pocket confined by H11, H20, H27 and S17 (Figure 21e). The hydrophilic side of tetracycline interacts with the phosphate-sugar backbone of residues 894/895 in the switch region of H27, and with the bulged bases U244, C245 and A246 of H11. Base G761 in H20 defines the other side of the pocket. Residues 99-101 in the C-terminal extension of S17, which is unique to thermophilic bacteria, are also involved in the binding. This site was revealed biochemically in mesophilic bacteria, therefore it seems that the C-terminal tail of S17 is not essential for the binding of tetracycline at this site.

Tet-6 is located in the vicinity of the E-site, in a cavity defined by Arg4 and Arg5 at the N-terminal end of S7, Arg120 of S9, and the helices H28, H34, H38, and H43 of 16S rRNA (Figure 21d). The interactions between rRNA and Tet-6 site are exclusively with the backbone of the RNA and are co-ordinated by a Mg^{2+} ion in a similar fashion to that observed for the Tet-1 site. These interactions involve residues G933 and C934 of H28, G1186 in the single-strand connecting H34 and H38, and U1345, and A1346 in the E-loop of H43. Overall, the binding of tetracycline to the Tet-6 site is dominated by the interaction of tetracycline with single stranded 16S RNA regions and the apparently flexible extensions of S7 and S9. Thus, the stability of the tetracycline bound at Tet-6 and hence its occupancy could vary according to the experimental conditions as indicated by biochemical data (Oehler et al., 1997). Although, Tet-6 is the site with the lowest relative occupancy, it can be correlated with many biochemical results (Table 4).

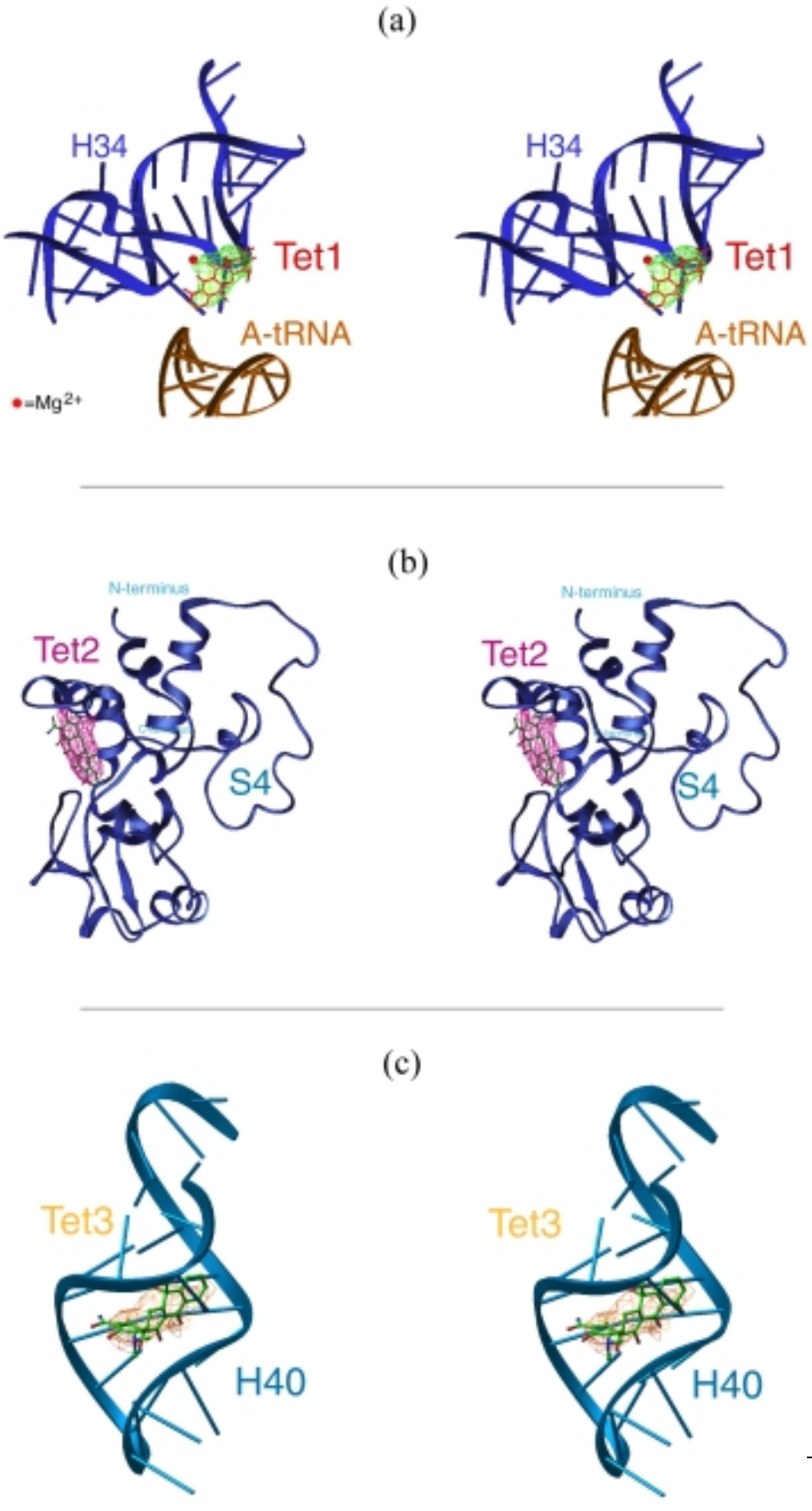
(a)
H34
Tet1
A-tRNA
●=Mg2+
H34
Tet1
A-tRNA
(b)
N-terminus
Tet2
S4
N-terminus
Tet2
S4
(c)
Tet3
H40
Tet3
H40

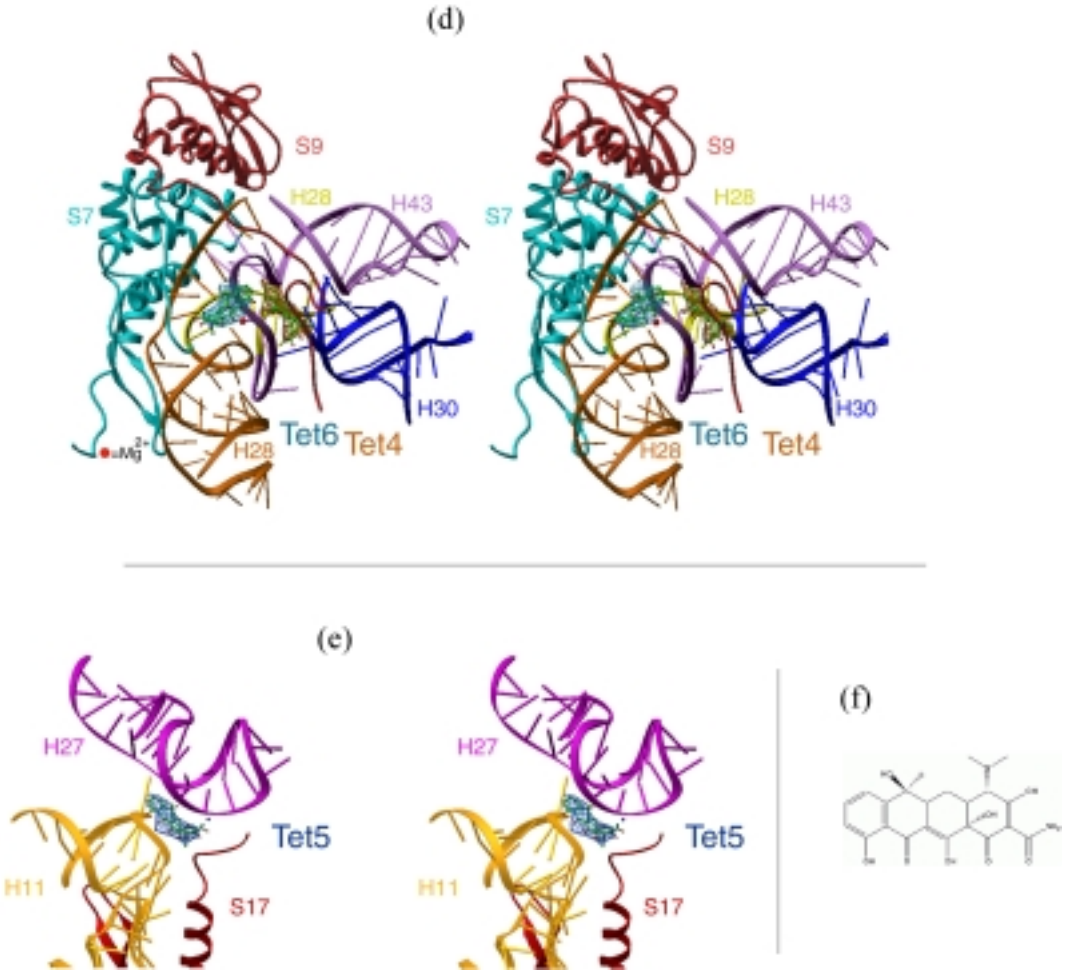

Figure 21. *Details of the binding sites of tetracycline.*

All images show the sigmaA weighted difference density at contour levels ranging from 3.2 to 2.2 sigma. (a) Stereo view of Tet-1. (b) Stereo view of Tet-2. (c) Stereo view of Tet-3. (d) Stereo view of Tet-4 and Tet-6. (e) Stereo view of Tet-5. (f) Chemical structure of tetracycline.